EARTHQUAKE ENGINEERING AND STRUCTURAL DYNAMICS
Earthquake Engng. Struct. Dyn. **28**, 371–391 (1999)

SIMULATION ANALYSES OF BUILDINGS DAMAGED IN THE 1995 KOBE, JAPAN, EARTHQUAKE CONSIDERING SOIL–STRUCTURE INTERACTION

YASUHIRO HAYASHI*, KAZUO TAMURA, MASAFUMI MORI AND IKUO TAKAHASHI
Izumi Research Institute, Shimizu Corporation, Japan

SUMMARY

A series of studies was conducted on three buildings of steel reinforced concrete structures with RC shear walls damaged in the 1995 Hyogo-ken Nanbu earthquake. These buildings are located in an area where structural damage centred around. Two of these buildings suffered severe damage, while the third was not structurally damaged. Our studies deal with site inspections, including micro-tremor measurement of buildings, the evaluation of input motions, and the response analyses considering soil–structure interaction. The results of simulation analyses of the two severely damaged buildings correspond to their actual damage state. From the response analyses of the one slender building with no structural damage, it was concluded that uplifting is the main reason it did not suffer any structural damage. Through these studies, the importance of soil–structure interaction and effective input motion is fully understood. Copyright © 1999 John Wiley & Sons, Ltd.

KEY WORDS: 1995 Hyogo-ken Nanbu earthquake (Kobe earthquake); SRC structure; site damage inspection; input motion characteristics; simulation analysis; soil–structure interaction

1. INTRODUCTION

The 1995 Hyogo-ken Nanbu earthquake caused severe damage to the city of Kobe and the surrounding area. It is an important and essential point to clarify what characteristics the input motion of buildings had, and how the buildings responded, suffering damage or surviving the earthquake undamaged.

Only a few ground motions were observed in severely damaged area during the Hyogo-ken Nanbu earthquake. Therefore, many researchers have used the strong motion records at Kobe Meteorological Agency (JMA, in Figure 1) for simulation analyses of buildings. Although the peak values are more than 800 cm/sec^2 in acceleration, and 90 cm/s in velocity, building damage was not severe around the JMA station. Therefore, JMA records were not appropriate as input motions for the simulation of building damage in the area with the most severe damage. Kawase and Hayashi (1995) evaluated ground motions in the most heavily damaged area of Chuo-ward, Kobe, showing consistency with observed records for the area. The estimated peak

* Correspondence to: Yasuhiro Hayashi, Izumi Research Institute, Shimizu Corporation, 2-2-2 Uchisaiwai-cho, Chiyoda-ku, Tokyo 100-0011, Japan. E-mail: hayashi@ori.shimz.co.jp

CCC 0098–8847/99/040371–21$17·50

Received 25 July 1997
Revised 19 January 1998 and 24 June 1998

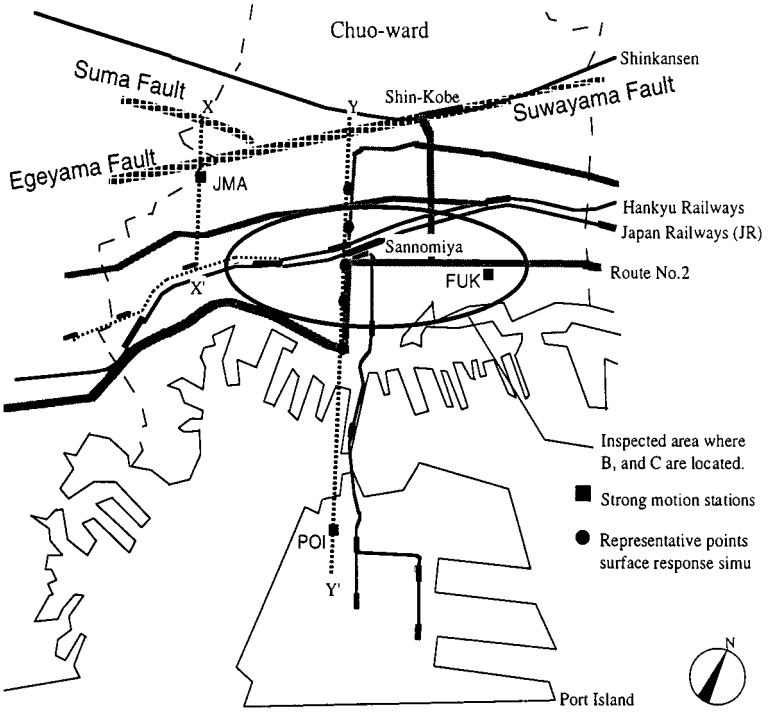

Figure 1. Map of Chuo-ward, Kobe city

ground velocity values were more than 100 cm/sec (see Figure 5(b)). In order to explain contradictions in seismic force level between input motions for simulation analyses and estimated motions, some researchers have pointed out that the effective input motions to buildings would be smaller than observed or estimated ground motions due to the soil–structure interaction effects. However, we can find only a few examples evaluating the effective input motions.

While most simulation analyses have been conducted on severely or moderately damaged buildings, it is also important to explain what factors distinguished buildings experiencing severe damage from those receiving no structural damage under strong ground motions. Therefore, we should examine the relationship between building damage and ground motions from many aspects.

In this paper, we describe a series of studies on damaged buildings due to the Hyogo-ken Nanbu earthquake. We inspected many buildings in Kobe city shortly after the earthquake, conducting simulation analyses for several of them, to examine their responses. The results from three of the buildings were selected and are introduced in this paper because we feel that the soil–structure interaction effects played an important role in accounting for the differences in damage levels. All three are composed of steel reinforced concrete (SRC) frames and RC shear walls, and are located in Chuo-ward of Kobe, where structural damage was centred (Figure 1). Two of the buildings suffered moderate to severe damage, and the other was not damaged in the structure.

Since buildings damaged in an earthquake should be examined from an overall point of view, our study includes damage inspection of the buildings at the sites, micro-tremor measurements,

evaluation of input motions, and response analyses of the buildings. In the response analyses, we consider soil–structure interaction and the effective input motions to the buildings to examine their effects on the building damage level.

2. OUTLINE OF THE SUBJECT BUILDINGS AND THEIR DAMAGE

All three buildings are office buildings located in the heavily damaged area of Chuo-ward, Kobe and are listed in Table I. Liquefaction was not observed around these buildings. 'Building A' has 13 storeys above ground and two below, 'Building B' 11 storeys above ground and one below, and 'Building C' 9 storeys above ground and one below. These three buildings have spread foundations, and superstructures are composed of SRC moment-resisting frames with RC shear walls. Many SRC buildings suffered the collapse of a mid-height storey during the earthquake. In many of these, the core of the SRC members were formed by a built-up steel section with angles or batten plates arranged to form lattices[1] as shown in Figure 2(a). Earlier research has demonstrated that SRC members with built-up steel web forming a lattice have lower shear strength than those fabricated with full steel web (rolled section as shown in Figure 2(b)), and show much deterioration for the interstorey drift angle in the order of 1 per cent.[2] Therefore, a 1975 revision to the SRC Building Code (AIJ SRC Standard Version 3)[2] recommended that full web steel be used. In the three buildings, full web steel was used for the core of SRC columns and girders. In estimation as described later (see Figures 12 and 15), the maximum interstorey drift angles for the three buildings are considered to be 1·0–1·5 per cent during the earthquake. In the

Table I. Outline of buildings

	Plan	Height	Number of stories	Damage to structure
A	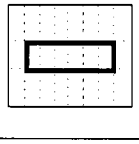 34m × 44m	49m	B2-13-P2	(Moderate damage) Shear cracks of RC shear walls of 4th ~ 6th floors were noticeable, especially in the north-south direction. Damage to other parts was slight.
B	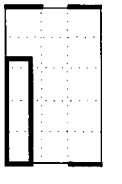 44m × 22m	41m	B1-11-P1	(Severe damage) Shear cracks of RC walls of 2nd ~ 7th floors were noticeable, especially in the north-south direction. Some of columns at the 2nd floor were damaged in bond-splitting or were slightly damaged in flexure.
C	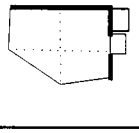 10m × 12m	31m	B1-9-P1	(Slight damage) Slight cracks occured in non-structural RC walls. There was no structural damage.

B : Basement, P : Penthouse

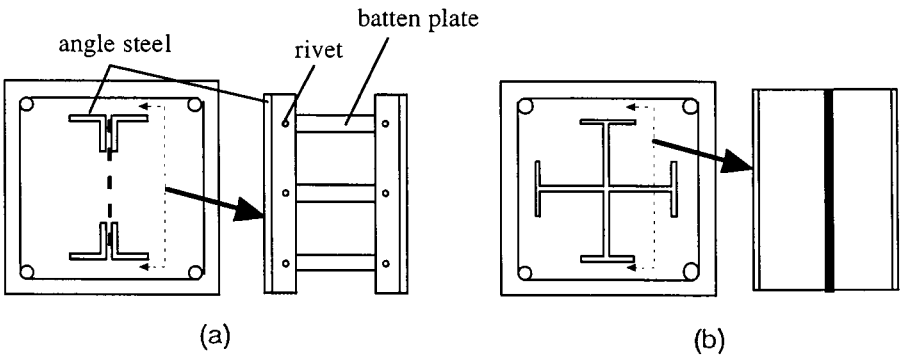

Figure 2. Typical SRC column sections: (a) built-up steel web forming a ladder; (b) full web steel (Buildings A, B, and C)

three buildings, SRC members were not severely damaged at all as described below. Therefore, the recommendation by the AIJ SRC Standard was successful for the three buildings.

Building A was built after 1981, when the Building Standard Law Enforcement Order was revised to its current format[3] which requires estimation of existing horizontal load resisting capacity at the formation of mechanism. This building has a set back in two directions at the third storey. The plan shape of the building is rectangular, with almost no structural eccentricity. A lot of large shear cracks were observed in RC shear walls around the elevator core. Damage was especially severe at the 4th–6th floors. However, the columns which support the weight of the building were not damaged at all.

Building B was built before 1981 and the plan shape of this building is also rectangular. This building does not have set back but the length of the transverse direction below ground is longer than those above ground. The RC core walls are laid out at one side of the floor plan. Shear walls were completely destroyed at the 2nd–7th floors; nevertheless, the supporting columns were not severely damaged.

Building C was built after 1981 and has a five-cornered plan shape, with the length of the transverse direction about 10 m. The foundation is embedded at 6 m depth and the height of the building reaches about 30 m above ground. Therefore, the building is slender. This building suffered no structural damage except for some hair cracks on a non-structural RC wall around the elevator shaft. However, gaps about 1–3 cm wide were observed between underground exterior walls and the surrounding soil, implying that separation between the foundation and the soil occurred during the earthquake.

In Buildings A and B, structural damage was dominant in the RC walls of the north–south (NS) direction when compared with the orthogonal (east–west; EW) direction. It should be noted again that vertical load-carrying systems in the two buildings were not severely damaged, and that the response energy was absorbed by the RC walls in compensation for their damage condition.

We conducted micro-tremor measurements on both damaged and undamaged buildings, including the Buildings A–C described above. Figures 3(a) and 3(b) show fundamental periods and their damping factors obtained from the micro-tremor measurement, respectively. Empty symbols ○, △ are the results for buildings with severe or moderate damage, and solid symbols ●, ▲ are the results for buildings with slight or no damage. In these two figures, results for RC and

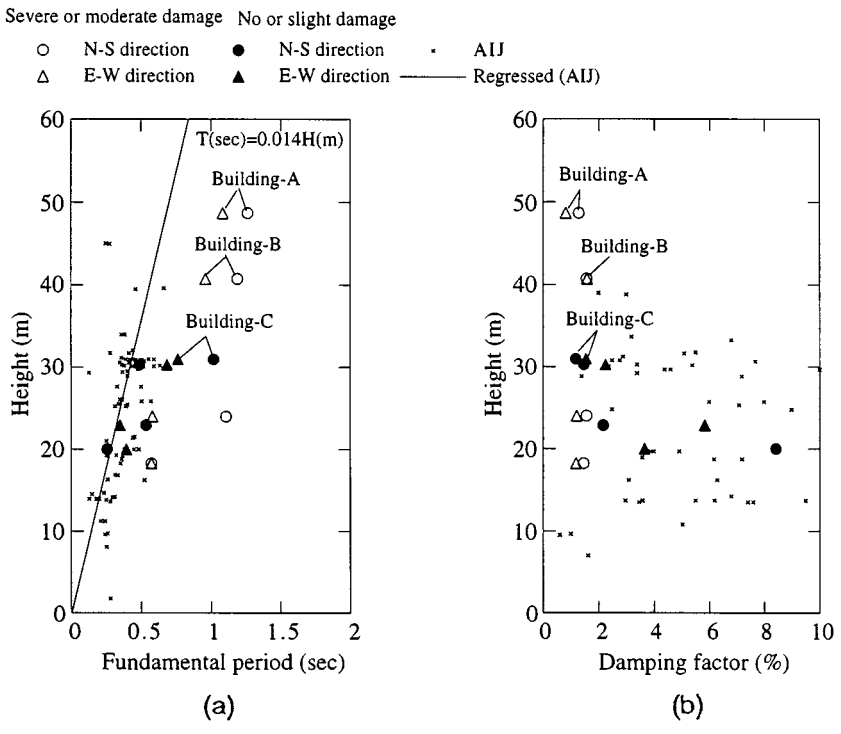

Figure 3. Fundamental periods and damping factors of damaged buildings: (a) fundamental period; (b) damping factor

SRC buildings measured immediately after construction by other researchers and edited by the Architectural Institute of Japan (AIJ) are also plotted. From Figure 3(a), it is apparent that fundamental periods for the buildings with severe and moderate damage are longer than those for normal buildings. Besides that, in the case of severely and moderately damaged buildings, including Buildings A and B, fundamental periods for the NS direction are longer than those for the EW direction. This is consistent with the fact that damage to buildings, and seismograms observed at the stations in Chuo-ward are predominant in the NS direction. Therefore, we simulated the response of damaged buildings in the NS direction. It must also be pointed out that damping factors for buildings with severe and moderate damage are smaller than those for buildings with no or slight damage as shown in Figure 3(b).

3. EVALUATION OF EARTHQUAKE INPUT MOTION

There were few observed ground motions around Chuo-ward in Kobe which was one of the most severely damaged areas during the Hyogo-ken Nanbu earthquake. Therefore, we adopted horizontal ground motions in the N30°W direction simulated by Kawase and Hayashi (1995),[4–6] as input motions to the buildings in this study. Details of the evaluation procedures they used for the ground motions and their characteristics are found in the references while an outline appears below.

Kawase and Hayashi inverted bedrock motions for the outcrop of nearby Rokko granite from the strong motion records at JMA (see Figure 1). They used an appropriate deep ground structure represented by a two-dimensional finite element model along X–X′ section in Figure 1. Then, they simulated the ground motions on the outcrop of the Osaka Group formation, the early Pleistocene layers, by using a 2-D finite element model which represented the geological structure beneath the central district of downtown Kobe (Y–Y′ section in Figure 1). Figure 1 shows the locations of the sections where ground motions were computed. Figures 4(a) and 4(b) show the finite element models representing the deep basin structures along the JMA section (X–X′ section) and Sannomiya section (Y–Y′ section), respectively. The Sannomiya section crosses the heavily damaged area. Ground surface motions were evaluated using simulated outcrop motions obtained along the Sannomiya section as input motions for the local shallow subsurface layer soil models. In the simulation analysis of surface response, they used a 1-D nonlinear effective stress analysis method[7,8] which took into account dynamic non-linear behaviour of the soil, including the increase of excess pore water pressure and cyclic mobility. The estimated

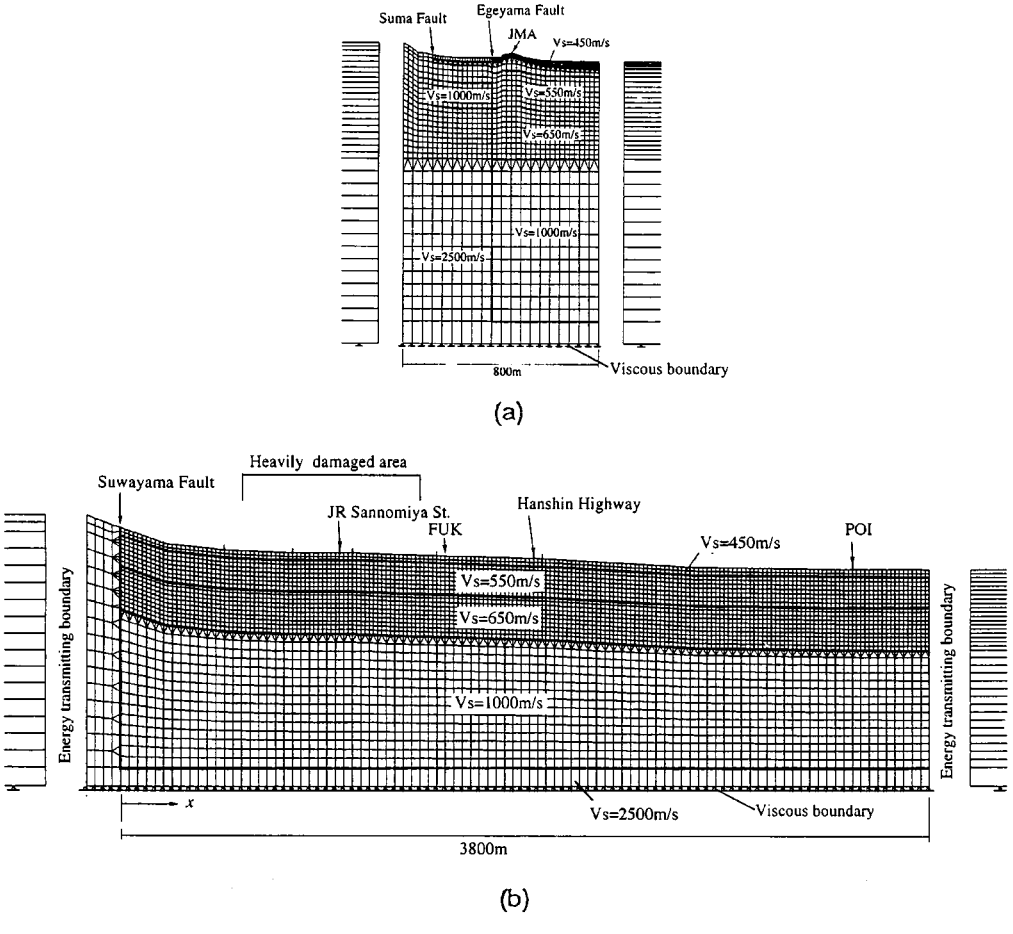

Figure 4. FEM models of ground: (a) X–X′ section; (b) Y–Y′ section

motion at the surface shows good agreement with observations at the FUK and POI stations shown in Figure 1. Furthermore, the distribution of maximum accelerations and velocities along the Sannomiya section agreed well with the 'damage belt' in Kobe as shown in Figure 5. They concluded that their evaluation was quantitatively reasonable to explain the overall damage in Kobe.

We calculated the equivalent velocities V_E $(= (2E_T)^{0.5})$ obtained from the total input energy[9] E_T to the 1-DOF system with natural period $T = 0{\cdot}5$, $1{\cdot}0$, and $2{\cdot}0$ s and with damping factor $h = 0{\cdot}1$. Figure 6(a) has the equivalent velocities for the outcrop of the Osaka group formations and Figure 6(b) indicates those for the observed (POI) or evaluated free ground surface motions. It is clear that the total input energy is very large in the heavily damaged area, especially for buildings with $T = 1{\cdot}0$ s. In the liquefied area, the total input energy decreased on the ground surface compared with the outcrop of Osaka group formations. This feature is obvious for the buildings with $T = 0{\cdot}5$ s, and this may be a cause for the reduction in building damage in the liquefied area.

We use the estimated outcrop motions described above as input motions to the hard soil layer of the soil model for simulation analysis of the buildings. Figures 7 and 8 show the

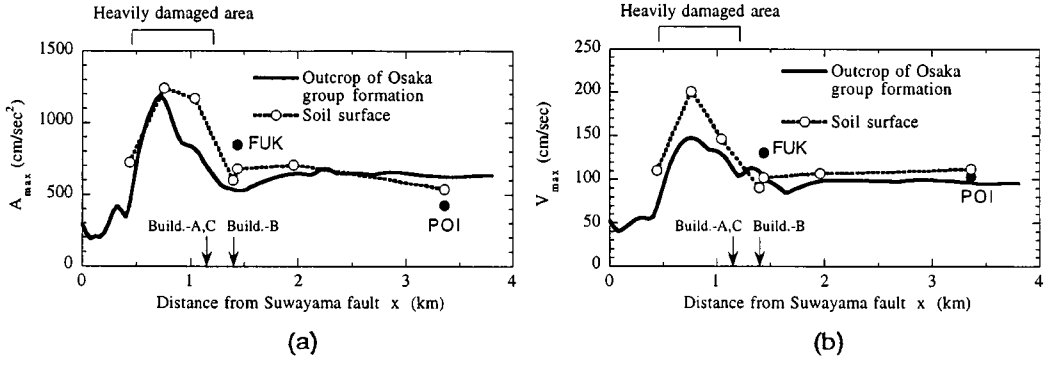

Figure 5. (a) Peak ground accelerations; and (b) velocities

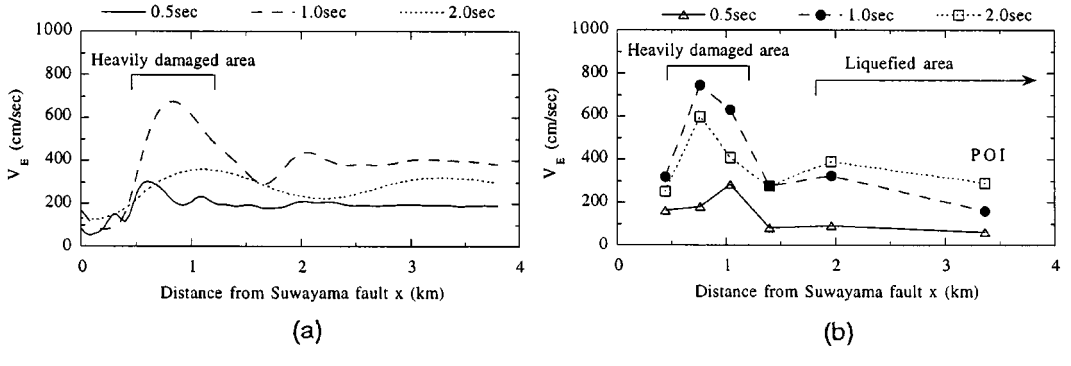

Figure 6. Equivalent velocities to the total input energy: (a) out crop motions of Osaka group formations; and (b) soil surface

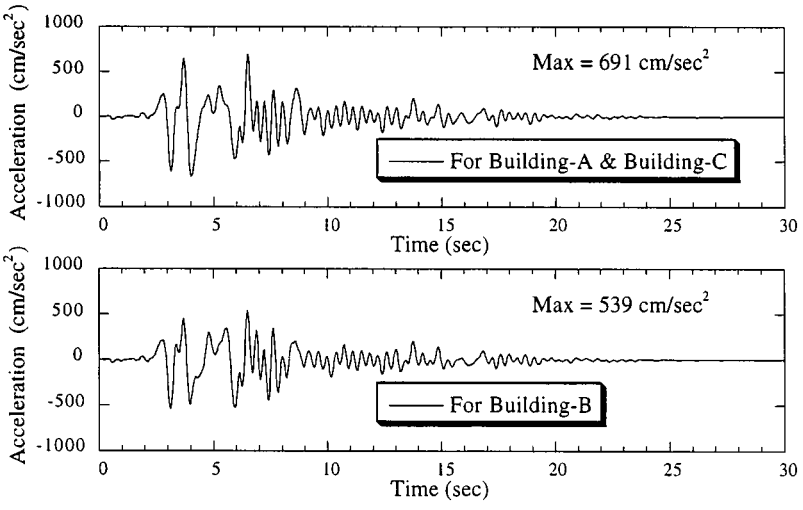

Figure 7. Simulated ground motions on Osaka Group formation ($V_s = 450$ m/s)

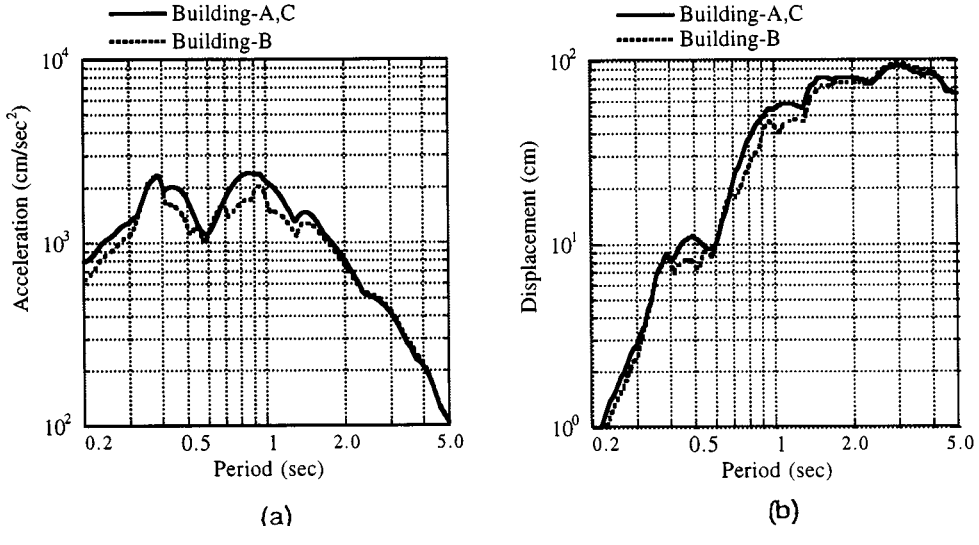

Figure 8. Response spectra ($h = 0{\cdot}05$) of estimated ground motions: (a) maximum acceleration; (b) maximum displacement

estimated input motions and their response spectra for the sites of Buildings A–C. The peak acceleration at the sites of Buildings A and C was about 690 cm/s^2, and about 540 cm/s^2 for Building B, but the peak velocity at the three sites was about 110 cm/s. Figure 8 shows that the response properties in the frequency domain for the two points are almost the same.

4. ANALYSIS MODEL

We have used sway-rocking models (SR models) with embedment. The buildings are modelled by multi-lumped-mass systems. Table II denotes weight, linear stiffness of shear springs and ultimate lateral strength of the buildings. The linear stiffness of the shear springs for Buildings A or B was evaluated with a static analysis in which design lateral loads were applied to a three-dimensional structural model with fixed foundation. For Building C, we adopt the stiffness calculated by the D-value method[10] because the structure is very simple. The D-value method is a simple and practical structural analysis method which is also described in the AIJ RC standard.[11]

The non-linear characteristics of the shear springs of Buildings A and B were assumed to be the trilinear type (see Figure 9) because this type is often applied to the analysis of SRC structures with full web steel cores.

According to the current Building Standard Law of Japan, the ultimate lateral strength coefficient C_{y0} of Buildings A or C had been calculated at the structural design stage. In addition, the ultimate lateral strength coefficient (C_{y1}) can also be evaluated from the design drawings using the second screening method in 'Standards for seismic performance evaluation of existing reinforced concrete buildings.[12]' Thus, $C_{y0} = 0{\cdot}52$ and $C_{y1} = 0{\cdot}62$ at the fourth storey of Building A. The C_{y0} is adopted for the response analysis. Furthermore, we performed sensitivity analyses varying non-linear hysteresis type and control parameters to define skeleton curve, variables such as R_y, Q_c/Q_y, and Q_y as is shown in Figure 9. However, our results suggested that sensitivity parameters, except for stiffness after yielding, were not so important to explain actual overall damage state. As for Building B, the ultimate lateral strength was based on C_{y1}, which was 0.66 at the severely damaged second floor. As for Building C, $C_{y0} = 0{\cdot}49$ and $C_{y1} = 0{\cdot}77$ at the first floor. The C_{y0} is far smaller than C_{y1} since non-structural walls were neglected in evaluating the ultimate lateral strength coefficients C_{y0} at the design stage. Consequently, the ultimate lateral strength coefficients are approximately 0·5–0·6 at the lower floors of Building A, 0·7 at the lower floors of Building B, and 0·8 at the 1st floor of Building C, respectively. Building strength does not distinguish clearly severe damage from no structural damage.

The soil–structure interaction springs calculated in the frequency domain were attached at their respective basements. Backfill was modelled with the Novak's spring[13] by replacing the rectangular foundation with an equivalent circular one in area. The subgrade was modelled with a horizontal spring and a rotational spring in which soil layering was precisely considered[14] assuming a rigid base. Bottom-level depths for the foundations were GL-11·9 m for Building-A, GL − 7·4 m for Building B, and GL-6·0 m for Building C, respectively. Foundation dimensions along and normal to the NS direction were about 60 and 56 m for Building A, 52 and 22 m for Building B, and 10 and 12 m for Building C, respectively.

Soil properties were evaluated from bore hole data and the equivalent linear soil model was assumed using a representative relationship between stiffness and shear deformation along with the damping ratio and shear deformation according to soil type.[15] Because liquefaction was not observed around the buildings, we used the simulated outcrop of the Osaka Group formations ($V_s = 450$ m/s) described in Section 3 (Figure 7) for input motions to the base layer of the soil analysis models. Soil profiles at the sites of the three buildings are shown in Tables III–V.

Damping types for the SR models are shown in Figure 9 and the damping coefficient for each structure is assumed to be proportional to its stiffness with the damping factor corresponding to the first mode of the structure–foundation system assumed to be 0·03. Damping of the soil–structure interaction spring can be treated as a combination of hysteretic damping of the soil

Table II. Analysis models for superstructures

(a) Building A

Floor	Level (m)	Weight (t)	Stiffness (t/cm)	Strength Q_y (t)
R	48·1	2280		
			2630	2670
13	44·5	1160		
			3250	3550
12	40·9	1160		
			3790	4110
11	37·3	1160		
			4290	4690
10	33·7	1160		
			4760	5240
9	30·1	1160		
			5230	5680
8	26·5	1160		
			5720	6110
7	22·9	1160		
			6310	6480
6	19·3	1160		
			6930	6510
5	15·7	1160		
			7690	6650
4	12·1	1160		
			8930	6790
3	8·5	3470		
			15 490	6790
2	4·8	3220		
			15 700	6890
1	0·0	4650		
			∞	∞
B1	− 4·3	4980		
			∞	∞
B2	− 8·9	13200		

(b) Building B

Floor	Level (m)	Weight (t)	Stiffness (t/cm)	Strength Q_y (t)
11	36·3	1840		
			4500	5270
10	32·3	1060		
			5950	5500
9	28·9	1030		
			6480	5500
8	25·5	1020		
			7400	5740
7	22·1	1030		
			7820	5740
6	18·6	1080		
			8540	6010
5	15·1	1110		
			9020	6010
4	11·6	1130		
			9890	6370
3	8·1	1090		
			10 200	6970
2	4·5	1160		
			7820	9370
1	0·0	1390		
			∞	∞
B1	− 4·2	1750		

(c) Building C

Floor	Level (m)	Weight (t)	Stiffness (t/cm)
R	31·0	291	
			213
9	27·7	190	
			208
8	24·3	195	
			189
7	21·0	193	
			243
6	17·6	193	
			247
5	14·3	197	
			257
4	10·9	205	
			284
3	7·5	208	
			308
2	4·0	223	
			241
1	0·0	267	
			∞
B1	− 4·0	582	

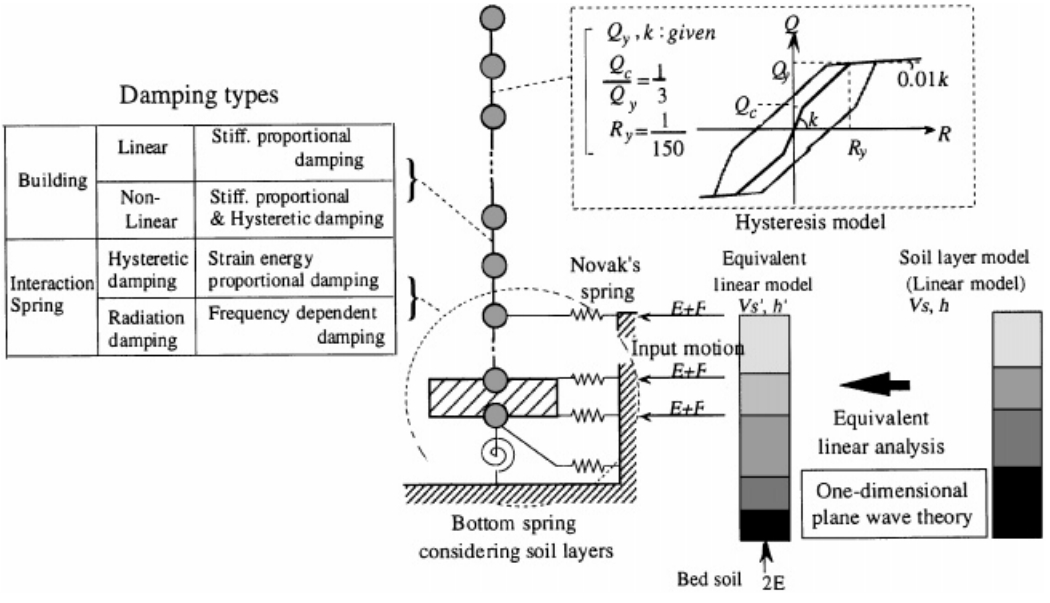

Figure 9. Analysis models for structure and foundation

and radiation damping to the soil for the sake of time-domain non-linear response analyses. The dynamic stiffness of soil springs $K(\omega)$, whose real part and imaginary part are $K_R(\omega)$ and $K_I(\omega)$, can be given by

$$K(\omega) = j\{K_I(0^+)/K_R(0)\}K_R(\omega) + \{K_R(0) + j\omega C_r(\omega)\}, \tag{1}$$

where j is $(-1)^{1/2}$. The first term in equation (1) approximately corresponds to the hysteretic damping of the soil. The second term includes the static stiffness $K_R(0)$ and residual dynamic stiffness $j\omega C_r(\omega)$, representing the effects of radiation damping. The first term is included in the damping coefficient matrix of the soil–structure interaction model as the modal damping matrix. The modal damping factor h of a mode is given by

$$h = (\Sigma W_i h_{ei})/(\Sigma W_i) \tag{2}$$

where W_i and h_{ei} are the strain energy and damping factor of an element i, respectively, and for the soil springs, $h_{ei} = K_I(0^+)/(2K_R(0))$. On the other hand, we evaluated the interaction force $R(t)$ in the time domain corresponding to the second term in equation (1) with the rigorous method[16] proposed by Hayashi and Takahashi. The method mentioned above can simulate frequency-dependent characteristics of $C_r(\omega)$ in the time domain efficiently and accurately.

Generally speaking, the predominant period of the soil and building system becomes lengthened and a hysteretic damping of the surface soil layer gets larger as shear strain increases (see Tables III–V) under large acceleration input. Therefore, the effects of hysteretic damping becomes dominant over radiation damping.

Building C was analysed paying attention to the fact that there was no damage to the building although it was located near Buildings A and B, which suffered severe structural damage. We used

Table III. Soil profile for Building A

	Layer no.	Depth (m)	Soil type	Unit weight γ (t/m^3)	Poisson's ratio v	Linear model		Equivalent linear model		
						Shear wave velocity V_s (m/s)	Damping factor h	Shear wave velocity V_s' (m/s)	Damping factor h'	Max. strain (per cent)
	1	0–1·7	Silty sand	1·8	0·45	150	0·03	112	0·12	0·055
	2	1·7–3·1	Fine sand	1·8	0·45	250	0·03	192	0·11	0·053
Foundation level	3	3·1–8·3	Coarse sand	1·8	0·45	415	0·03	344	0·08	0·039
GL-11·9 m	4	8·3–11·9	Fine sand	1·8	0·45	270	0·03	162	0·13	0·30
	5	11·9–13·1	Fine sand	1·8	0·45	345	0·03	228	0·11	0·18
Water level GL-13·1 m	6	13·1– ∞	Fine sand	1·8	0·45	450	0·03	450	0·03	—

Table IV. Soil profile for Building B

	Layer no.	Depth (m)	Soil type	Unit weight γ (t/m^3)	Poisson's ratio v	Linear model		Equivalent linear model		
						Shear wave velocity V_s (m/s)	Damping factor h	Shear wave velocity V_s' (m/s)	Damping factor h'	Max. strain (per cent)
Water level GL-2·5 m	1	0–2·5	Fine sand	1·8	0·45	210	0·03	167	0·11	0·034
	2	2·5–7·4	Coarse sand	1·8	0·45	320	0·03	232	0·12	0·069
Foundation level	3	7·4–13·5	Silty sand	1·8	0·45	245	0·03	134	0·14	0·42
GL-7·4 m	4	12·5–17·5	Sandy silt	1·8	0·45	210	0·03	82	0·18	1·43
	5	17·5–20·0	Coarse sand	1·8	0·45	325	0·03	178	0·15	0·36
	6	20·0– ∞	Coarse sand	1·8	0·45	450	0·03	450	0·03	—

Table V. Soil profile for Building C

	Layer no.	Depth (m)	Soil type	Unit weight γ (t/m^3)	Poisson's ratio v	Linear model		Equivalent linear model		
						Shear wave velocity V_s (m/s)	Damping factor h	Shear wave velocity V_s' (m/s)	Damping factor h'	Max. strain (per cent)
Foundation level	1	0–3·5	Coarse sand	1·8	0·45	250	0·03	184	0·13	0·055
GL-6·0 m	2	3·5–6·0	Coarse sand	1·8	0·45	315	0·03	219	0·12	0·1
	3	6·0–7·6	with gravel	1·8	0·45	315	0·03	243	0·08	0·12
Water level GL-7·6 m	4	7·6–12·7	Coarse sand	1·8	0·45	315	0·03	110	0·18	0·86
	5	12·7–15·6	Clayey sand	1·8	0·45	255	0·03	94	0·20	1·5
	6	15·6–18·7	Clayey sand	1·8	0·45	255	0·03	90	0·20	1·9
	7	18·7–∞	Fine sand	1·8	0·45	450	0·03	450	0·03	—

not only the SR model mentioned above but also a 2-D finite element model with joint elements[17] to analyse the basemat uplift and separation effect between the foundation and soil.

5. RESPONSE ANALYSES AND DISCUSSION

5.1. Response characdteristics of linear buildings and the soil

We show response characteristics for the three buildings and the soil using SR models with embedment and a fixed base model (model F) in Figure 10. As for the SR models, we assumed two scenarios: 'model L' in which the soil is linear, and 'model N' in which soil non-linearity is considered to be equivalently linear. Thus, we assumed all buildings to be linear. Figure 10 shows the amplification ratios for the buildings or the free field of the input motions mentioned above.

Figure 10(a) shows the responses at the roof of the buildings. Fundamental periods of fixed base models for Buildings A and B are 0·76 and 0·52 s, respectively. They agree well with average values for undamaged RC and SRC buildings in Figure 3(a). The fundamental period for the fixed base model for Building C is 1·1 s and this value is a good approximation of results from microtremor measurement. By comparing the fundamental peak frequencies and peak amplitudes of the three analysis cases, we can point out the following: variations in the fundamental frequency and its damping of Building A is small because the foundation is supported on a very stiff soil layer. For Buildings B and C, however, there were softer soil layers than the Osaka group formations under the foundations. In these soil layers, evident non-linearity appeared during the earthquake, namely, equivalent stiffness decreased and equivalent damping factors increased. Therefore, the peak frequency or its amplitude of Model-N becomes smaller than that of Model L or Model F.

Figures 10(b) and 10(c) show soil response and foundation response. From Figure 10(b), the predominant frequency of the non-linear soil model is much less than that of the linear soil model and variation in the peak frequency of the soil is drastic compared with that of the building. The foundation response of Buildings B or C around the predominant frequency of the building is amplified by the non-linear behaviour of the surface soil layer. For Building A, however, the foundation response is not affected by the non-linearity of the soil.

As we described above, the effects of soil–structure interaction and soil non-linearity are different for these three buildings. Nevertheless, the foundation response is almost equal to the free field motion at the foundation level around the predominant frequency of the buildings as shown in Figure 10(c). This suggests that free field motion at the foundation level is adequate for input to the fixed base model, Model F. In addition, the difference between foundation response and soil surface motion is not large around the predominant frequency of the buildings. Therefore, effective input motions to the three buildings are nearly equal to the soil surface motions.

5.2. Damage simulation for Buildings A and B

Figures 11 and 12 show the distribution of maximum accelerations and maximum interstorey drifts, respectively, for Buildings A and B. In the figures, results of four analysis cases are shown. The building models are assumed as linear or non-linear, and the effect of soil–structure

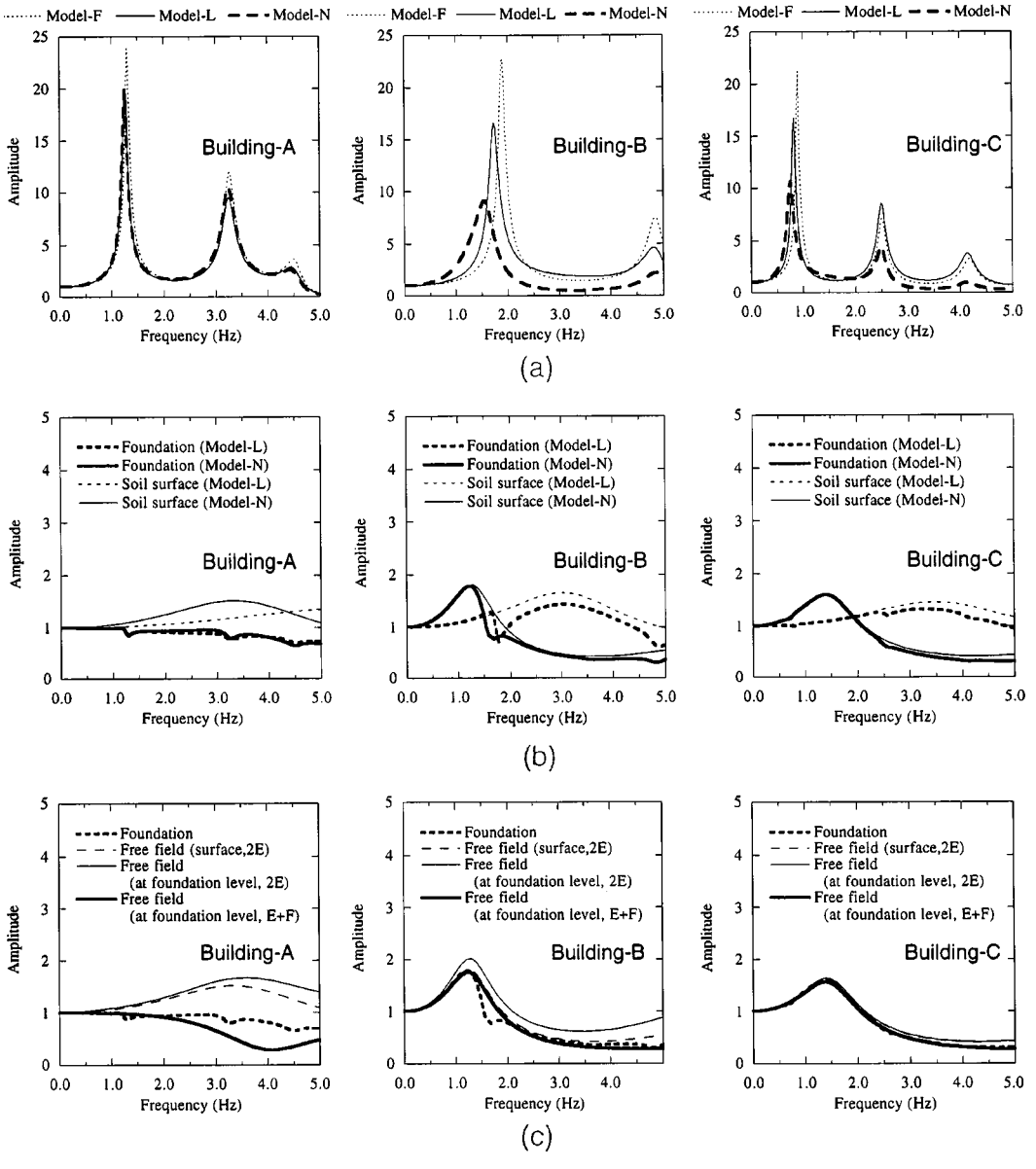

Figure 10. Response characteristics of buildings and surface soil layers: (a) roof of building; (b) foundation of building and soil surface; (c) comparisons between foundation and soil (Model N)

interaction is considered or it is neglected (fixed base models). For the fixed base models, the free field response ($E + F$) at the foundation level is used as an input. Response accelerations are higher than 1000 cm/sec^2 at the top floor, even in the non-linear models. This is reasonable when we consider the state of the rooms in the buildings, in which furniture was drastically moved or toppled.

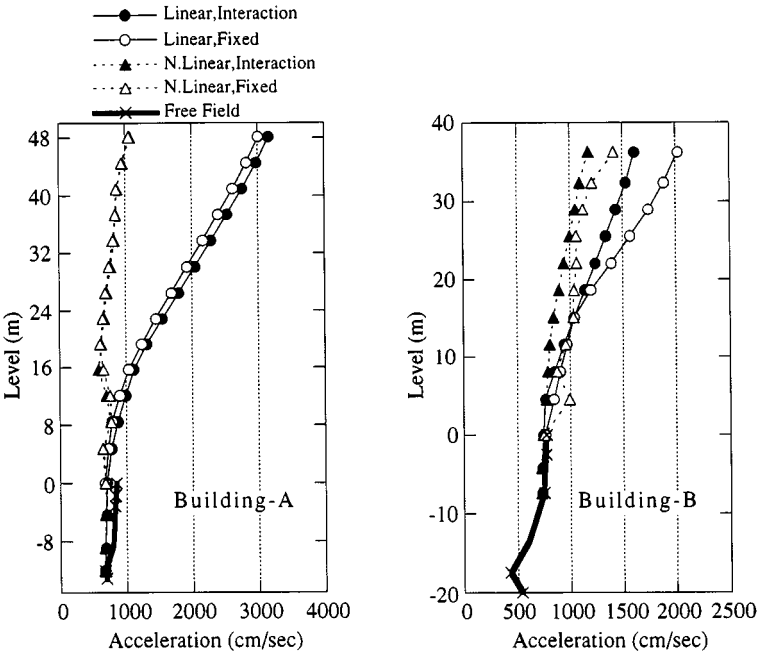

Figure 11. Maximum acceleration

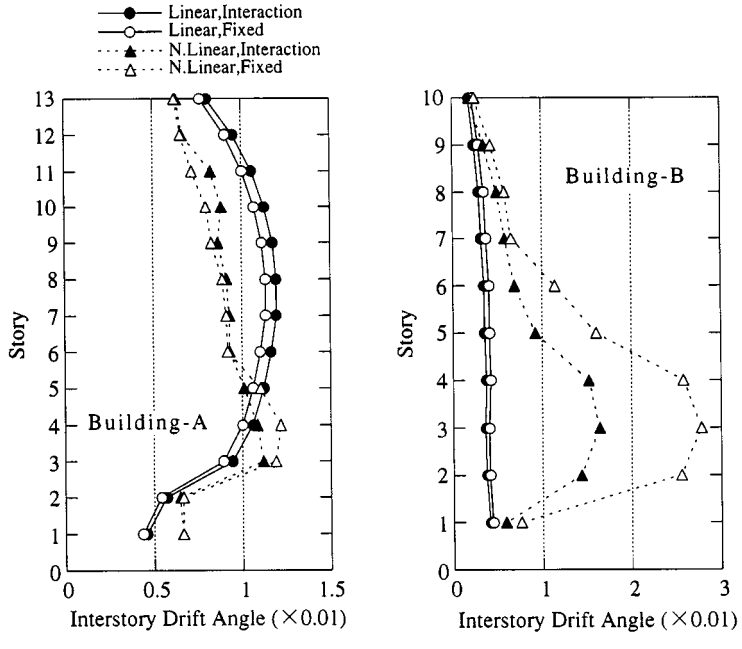

Figure 12. Maximum interstorey drift angles

In Figure 12, the maximum interstorey drift angle of Building B from non-linear analysis is five to ten times as large as that from linear analysis, although this phenomenon does not occur in Building A. This difference can be easily understood from displacement response spectra of input waves shown in Figure 8(b) and peak frequencies of linear response characteristics shown in Figure 10. Natural periods of Buildings A and B are approximately 0·9 and 0·6 s, respectively. Displacement response increases drastically with periods between 0·6 and 1·0 s. However, increase in displacement response over 1·0 s is not so large as that between 0·6 and 1·0 s. Therefore, when equivalent period becomes large with the development of non-linearity, increase in interstorey displacement for Building B becomes more conspicuous than that for Building A.

As mentioned in Section 2, both Buildings A and B suffered severe damage to structural members (mainly RC shear walls). The severest damage was observed at the 4th–6th floors for Building A, and at the 2nd–7th floors for Building B. Our response analysis results shown in Figure 12 correspond to this actual damage distribution and the maximum interstorey drift angles are approximately 1 per cent for Building A and 1–1·5 per cent for Building B. From these results it can be said that the strong seismic force of the Hyogo-ken Nanbu earthquake caused large shear cracks in RC shear walls in these two buildings.

From Figures 11 and 12, there seems no large difference in response distribution between the case where soil–structure interaction is considered and the case with free field response ($E + F$) was subjected to the fixed base model. Building B is an exception in that the non-linearity is remarkable, and there is a slight difference in interstorey displacement between the two models. The reason for this is that the SR model has a larger damping factor than the fixed base model by the soil–structure interaction effects.

5.3. Simulation for Building C with no structural damage

For Building C, we also conducted response analyses using the SR model with embedment (models L and N) and the fixed base model (model F). Figure 13 shows the distribution of the maximum response lateral force coefficients for models F, L, and N. The maximum response lateral force coefficient for the first floor is 1·9 for model F, 1·5 for model L and 1·2 for model N. The estimated lateral strength coefficient is about 0·8 at the 1st floor as mentioned before. Model F response is about twice as large as the estimated lateral strength while model N response is smaller than for models F and L. However, the results from model N cannot fully explain the actual state (no structural damage) of this building during the earthquake.

The maximum overturning moment obtained using the SR model was about nine times as great as the start-uplifting moment, which was calculated by assuming a linear normal stress distribution under the basemat. In addition, Building C has a slender shape and we found a gap between the underground exterior walls and the soil after the earthquake as mentioned previously. Therefore, it is possible that this basemat uplift occurred during the earth-quake. Thus, we used a 2-D FEM model with joint elements[17] to take into account the phenomena of the basemat uplift and separation between the underground exterior walls and the soil as shown in Figure 14. In this figure, the building model has linear springs and their underground stiffness is assumed to be rigid. The soil is to be equivalent linear and soil properties are shown in Table V. The bottom level of the FEM region is GL-22 m and viscous boundaries are attached to both sides and at the bottom, respectively, to account for outgoing waves. We used the simulated outcrop motion for the Osaka Group formations as input to the

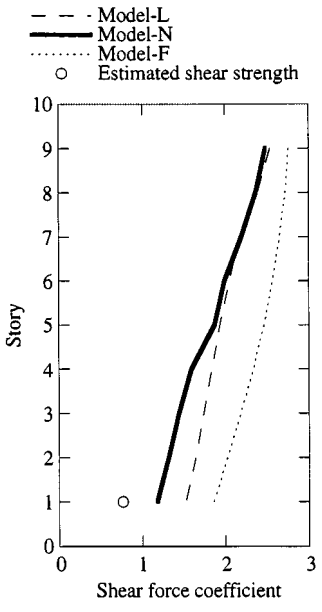

Figure 13. Maximum response shear force coefficients (with or without interaction by SR model)

bottom of the FEM and we carried out response analyses both with and without uplift using this model.

Figure 15(a) shows the distribution of maximum response lateral force coefficients, and the response of the model with uplift is about two thirds to half of that without uplifting. Therefore, the response level of the building reaches the same level as the ultimate capacity of the building when considering basemat uplift.

Figure 16 shows deformation at the time maximum base lateral force occurred. The whole building rotated from the bottom of the foundation. The thick lines with symbols in Figure 15(b) show the rotational angle at each floor, which is horizontal displacement from the ground level divided by the height of the floor from the ground level. The thin lines are rotational angles of the foundation. Rotational angles at each floor does not vary much between analysis cases, however, the rotational angle of the foundation drastically increased when considering basemat uplift. Therefore, interstorey deformation was reduced by increases in the foundation rotational angle. From this result, it can be concluded that the uplifting effect can be the main reason why the slender building did not suffer any structural damage. Sensitivity analysis on the damage reduction effect of basemat uplift has also been carried out and the effect is generalized in Reference.[18] The damage reduction effect of basemat uplift is valid for slender buildings whose basemat length is less than 20 m and the number of storeys is less than 15. Thus, we cannot expect this reduction effect for Buildings A and B. Additionally, we should note that the extent of reduction is completely different depending on the strength of buildings and the properties and intensity of input motions because reduction effects need conspicuous basemat uplift. For example, reduction effects will not appear when the strength of buildings and seismic force level are low to produce basemat uplift. Even if seismic force level is high, input motions have to had predominancy around 1 sec.

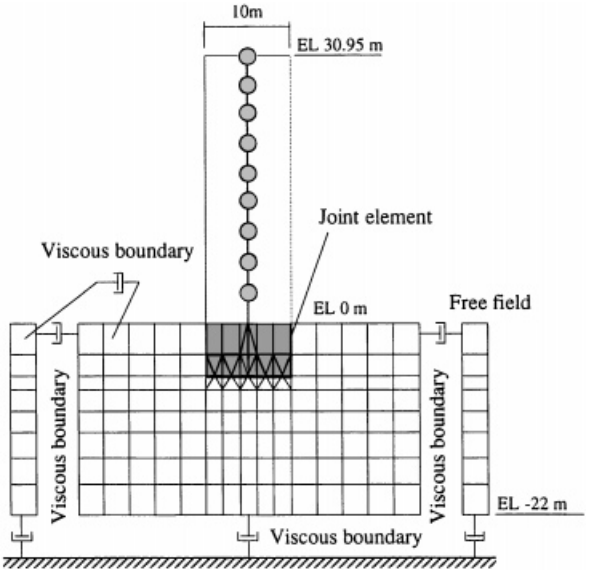

Figure 14. FEM analysis model

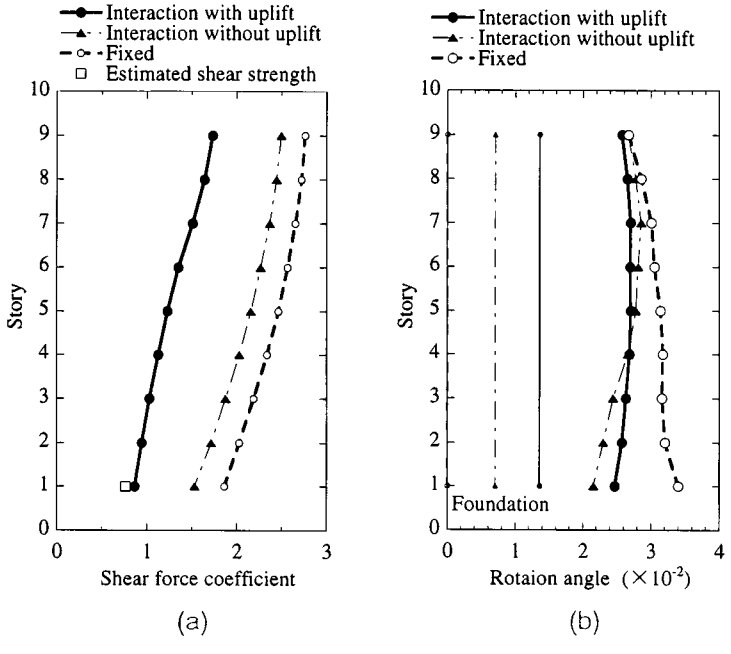

Figure 15. Maximum response (with and without uplift by 2-D finite element model): (a) shear force coefficient; (b) rotational angle

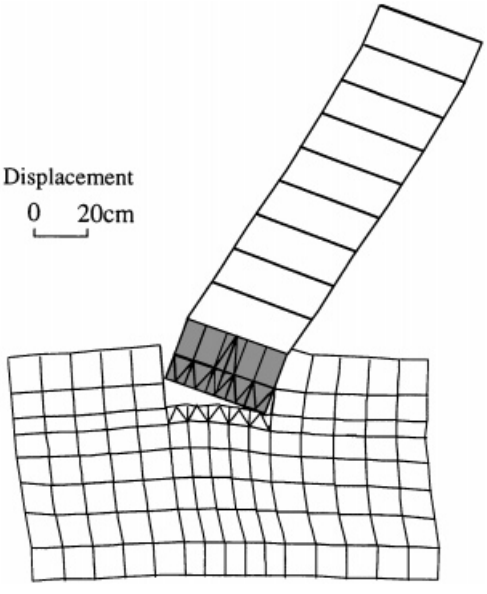

Figure 16. Deformation in uplifted state

6. CONCLUDING REMARKS

In this paper, a series of studies on the buildings damaged in the Hyogo-ken Nanbu earthquake has been described. The subject buildings were three steel reinforced concrete structures with RC shear walls, located at the centre of Kobe, where structural damage was concentrated. The study includes damage inspection and microtremor measurement of the buildings, evaluation of input motions, and response analyses, taking into consideration soil–structure interaction of the buildings.

Evaluated input motions for the simulation analyses of the three buildings showed good correspondence with observed records and overall building damage distribution in Kobe. Their peak velocities were about 110 cm/sec. The maximum interstorey drift angles were estimated to be more than 1 per cent for two of the buildings which suffered severe damage to their RC shear walls, that is, the simulation analysis results corresponded to their actual damage state. The strong seismic force of the earthquake caused the severe damage of the RC walls in these two buildings. However, SRC columns and girders with full web steel cores suffered no severe damage. In the Hyogo-ken Nanbu earthquake, many SRC buildings suffered the collapse of a mid-height storey; in many of these collapses, a built-up steel section formed the core of the SRC member. The built-up steel sections were often fabricated with angles arranged to form lattices or ladders. SRC members with built-up steel sections have lower shear strength than those fabricated with full steel webs and deteriorate even at the deformation angles of 1 per cent. Namely a 1975 revision to the AIJ SRC Standard which recommends the use of full web steel cores is shown to be appropriate for the Kobe earthquake. In addition, response energy was absorbed by the RC walls, compensating for their damage condition.

From the response analyses of a slender building which experienced no structural damage, using a 2-D FEM model taking basemat uplift into consideration, it was concluded that uplifting was the main reason why it did not suffer any structural damage.

In our study, the effects of non-linear soil–structure interaction and effective input motion were successfully used to evaluate the response characteristics of buildings subjected to very strong ground motions. In addition, free field motion at the foundation level was adequate as an effective input to a fixed base model for the sake of damage simulation.

ACKNOWLEDGEMENTS

The authors would like to express their gratitude to Mr. K. Watanabe and Dr. M. Kaneko of Izumi Research Institute, and Dr. H. Yokota and Mr. T. Saito of the Technical Institute of Shimizu Corporation for their cooperation in the inspection of buildings and response analyses.

REFERENCES

1. Architectural Institute of Japan, *Preliminary Reconnaissance Report of the 1995 Hyogoken-Nanbu Earthquake* (English edition), 1995.
2. Architectural Institute of Japan, *AIJ Standard for Structural Calculation of Steel Reinforced Concrete Structures*, 399–428 (1975) (in Japanese).
3. Building Center of Japan, *Structural Provisions for Buildings*, 1994 (in Japanese).
4. H. Kawase and Y. Hayashi, 'Strong motion simulation in Chuo-ward, Kobe, during the Hyogo-ken Nambu earthquake of 1995 based on the inverted bedrock motion', *J. Struct. Constr. Engng.* **480**, 67–76 (1996) (in Japanese).
5. Y. Hayashi and H. Kawase, 'Strong motion evaluation in Chuo-ward, Kobe, during the Hyogo-ken Nambu earthquake of 1995', *J. Struct. Constr. Engng.* **481**, 37–46 (1996) (in Japanese).
6. H. Kawase and Y. Hayashi, 'Strong motion simulation in Sannomiya, Kobe, during the 1995 Hyogo-ken Nambu Earthquake and its implication to structural damage', *Proc. 7th U.S.-Japan Workshop on the Improvement of Structural Design and Construction Practices*, Kobe, Hyogo-ken, Japan, (3-1)–(3-12), 18–20 January 1996.
7. K. Fukutake and H. Matsuoka, 'A unified law for dilatancy under multi-dimensional simple shearing', *Proc. Japan Soc. Civil Engng.*, 412/III-12, 1989, pp. 240–248 (in Japanese).
8. K. Fukutake, A. Ohtsuki, M. Sato and Y. Shamoto, 'Analysis of saturated dense sand–structure system and comparison with results from shaking table test', *Earthquake Engng. Struct. Dyn.* **19**, 977–992 (1990).
9. H. Akiyama, *Earthquake-Resistant Limit-State Design of Building*, University of Tokyo Press, Tokyo, 1985.
10. K. Muto, *Seismic Analysis Method* (Part 1), Maruzen, Corporation, 1963 (in Japanese).
11. Architectural Institute of Japan, *AIJ Standard for Structural Calculation of Reinforced Concrete Structures*, 1982 (in Japanese).
12. The Japan Building Disaster Prevention Association, *Standards for Seismic Performance Evaluation of Existing Steel Reinforced Concrete Buildings*, 1983 (in Japanese).
13. M. Novak, T. Nogami and F. Aboul-Ella, 'Dynamic soil reaction for plane strain case', *Proc. ASCE*, EM4, 1978, 953–959.
14. T. Sato, H. Kawase and K. Yoshida, 'Dynamic response analysis of rigid foundations subjected to seismic waves by boundary element method', *Proc. 5th Int. Conf. Boundary Elements*, 1983, pp. 765–774.
15. S. Yasuda and I. Yamaguchi, 'Dynamic soil properties of undisturbed samples', *The 20th Japan Conf. on Soil Mechanics and Foundation Engineering*, 1985, pp. 539–542 (in Japanese).
16. Y. Hayashi and I. Takahashi, 'An efficient time-domain soil–structure interaction analysis based on the dynamic stiffness of an unbounded soil', *Earthquake Engng. Struct. Dyn.* **21**, 787–798 (1992).
17. K. Toki, T. Sato and F. Miura, 'Separation and sliding between soil and structure during strong ground motion, *Earthquake Engng. Struct. Dyn.* **9**, 253–277 (1981).
18. Y. Hayashi, 'Damage reduction effect due to base mat uplift of buildings', *J. Struct. Constr. Engng.*, **485**, 53–62, July (1996) (in Japanese).

